Cell Proliferation Without Neurogenesis in Adult Primate Neocortex

David R. Kornack[1,2] and Pasko Rakic[1]*

A recent assertion that new neurons are continually added to the neocortex of adult macaque monkeys has profound implications for understanding the cellular mechanisms of higher cognitive functions. Here we searched for neurogenesis in adult macaques by using immunofluorescent triple labeling for the DNA-replication indicator, bromodeoxyuridine (BrdU), and neuronal and glial cell markers. Although numerous BrdU-labeled cells were distributed throughout the cerebral wall, including the neocortex, these were identified as nonneuronal cells; evidence for newly generated neurons was limited to the hippocampus and olfactory bulb. Thus, our results do not substantiate the claim of neurogenesis in normal adult primate neocortex.

Higher cognitive functions in primates, including humans, depend on the appropriate number, organization, and connectivity of neurons in the association areas of the neocortex (*1*, *2*). Studies with ^{3}H-thymidine (^{3}H-TdR) autoradiography, which labels DNA in dividing cells and their progeny, have indicated that neocortical neurons are generated before or shortly after birth in all species examined (*3*–*10*). In macaque monkeys, cortical neurogenesis occurs in a strict inside-to-outside (deep to superficial) laminar order before birth (*7*), whereas gliogenesis—in macaques as in other species—continues postnatally (*11*–*13*).

More recently, the generation of cells in the nervous system has been studied with the thymidine analog, 5-bromodeoxyuridine (BrdU), which also labels DNA during cell division (*14*). This method has been combined with cell-type–specific immunomarkers and confocal microscopic imaging to detect newly generated neurons in the adult hippocampus and olfactory bulb of rodents (*15*–*17*) and primates (*18*–*21*). With this approach, it was recently reported that considerable numbers of new neurons are continuously added to neocortical association areas during adulthood in macaque monkeys (*22*). The report further indicated that these neurons are produced in the subventricular zone (SVZ) of the lateral cerebral ventricles and then migrate in streams through the subcortical white matter to the prefrontal, posterior parietal and inferior temporal neocortex. Moreover, after reaching the neocortex within 2 weeks after their generation, the new neurons were reported to extend axons to other cortical areas (*22*) and then die within the next 7 weeks (*23*, *24*).

Because of the considerable conceptual and biomedical implications of this claim, it is essential to validate the reliability and robustness of this putative phenomenon. Accordingly, we examined the proliferation and phenotypic differentiation of cells in the cerebrum of adult macaque monkeys at various times after BrdU injections by using triple-label immunofluorescence for BrdU, glial fibrillary acidic protein (GFAP, a marker for astrocytes), and either NeuN (a marker for adult neurons) or class III β-tubulin (TuJ1, a marker for immature neurons) (*25*). We surveyed the prefrontal cortex—including the principal sulcus, where the majority of adult-generated neurons were reported—by examining every third section in a sequential series of coronal sections. The sections were first scanned with conventional epifluorescence microscopy with a dual-band filter set, which allowed simultaneous viewing of the fluorescence signals of BrdU and neuronal markers. All cells suspected of being double-labeled for BrdU and a neuronal marker were examined in detail with three-dimensional confocal analysis.

BrdU-labeled nuclei were observed in the neocortex of each monkey, irrespective of the particular injection schedule. The animals perfused 10 and 23 days after the final BrdU injection were most informative because these survival times correspond to the time point when adult-generated neurons are reportedly present in greatest numbers in the cortex before their demise. We found that many BrdU-labeled cells within the neocortex were distributed as "doublets" and were the likely daughter cells of a mitotic event within the neocortex (Fig. 1). The phenotype of BrdU-labeled cells in the cortex was examined with triple-label immunofluorescence histochemistry for BrdU, NeuN, and GFAP. Although we surveyed more than 1000 BrdU-labeled cells in the prefrontal neocortex in each monkey, in no instance did we find a BrdU-labeled cell that was colabeled with NeuN. This result differs markedly from the previous study (*22*), which claimed that 1 to 2 weeks after BrdU injections, 38 to 52% of the BrdU-labeled cells in the principal sulcus colabeled for NeuN. Given the number of BrdU-labeled cells that we surveyed in the principal sulcus alone, the probability of missing 38 to 52% [or even the revised, lower estimate of 25% (*24*)] of the total BrdU-labeled cell population as double-labeled neurons is infinitesimally small. This discrepancy may be due to differences in histological analysis [e.g., (*26*)] or other artifacts (*27*, *28*).

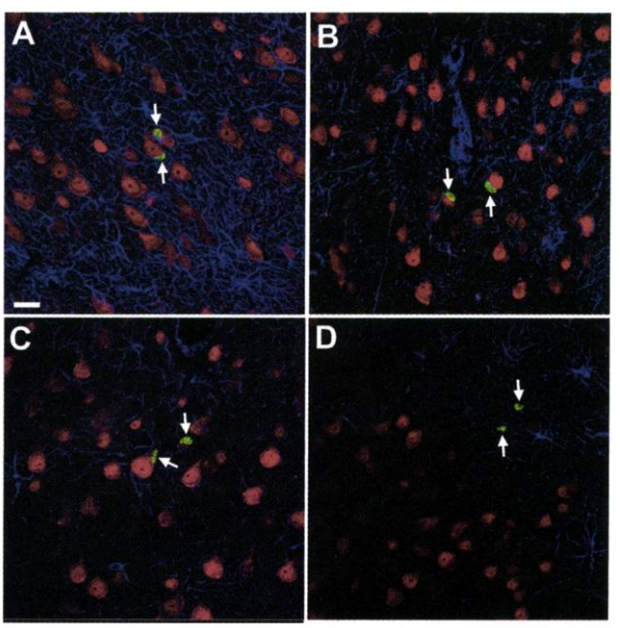

Fig. 1. Confocal microscopic images of BrdU-labeled cells in the frontal cortex of adult macaque monkeys. BrdU-labeled cells in cortex were often distributed as "doublets" (arrows), as illustrated by these examples in cingulate cortex (**A** to **C**) and prefrontal cortex (**D**) 10 days [(A) to (C)] and 32 days (D) after BrdU injections. BrdU-labeled nuclei (green) are closely associated with the perikarya of NeuN-positive neurons (red) but are not immunopositive for NeuN, indicating a nonneuronal phenotype. GFAP immunoreactivity (blue) indicates the presence of astrocytes. None of the neurons were labeled with BrdU. Scale bar, 20 μm for (A) to (D).

[1]Department of Neurobiology, Yale University School of Medicine, New Haven, CT 06510, USA. [2]Center for Aging and Developmental Biology, Department of Neurobiology and Anatomy, University of Rochester Medical Center, Rochester, NY 14642, USA.

*To whom correspondence should be addressed. E-mail: pasko.rakic@yale.edu

For example, upon initial inspection of our material, some BrdU-labeled nuclei appeared to belong to cortical neurons, which would be indicative of adult-generated neurons. However, in such cases, detailed confocal *z*-series analyses (i.e., examining sequential optical sections at intervals of 0.8 μm in the *z* axis) revealed that these BrdU-labeled nuclei actually belonged to cells that were closely apposed to neurons but were themselves immunonegative for NeuN (Fig. 2). The nuclei of NeuN-positive neurons were invariably immunonegative for BrdU (Fig. 2). Thus, the BrdU-labeled nuclei in these initially ambiguous cases appear to belong to newly generated satellite glial cells, which have been previously described in the neocortex of adult monkeys with both ^{3}H-TdR and BrdU methods (*29–31*) as well as in the cortex of other mammals (*11*, *12*, *26*, *32*).

Gould *et al.* have proposed that most of the putative new neurons in the monkey neocortex die within 9 weeks after being generated and that the previous ^{3}H-TdR autoradiography studies failed to detect them because of the longer survival periods used in these studies (*22–24*). However, in the present analysis, new cortical neurons were not detected even in the animals with short survival intervals. Even if, because of the sampling procedure or technical limitations, we have missed some BrdU-labeled neurons, their number would be exceedingly small. It would also be essential to exclude BrdU labeling resulting from DNA synthesis in response to cell damage, abortive mitoses, or initial steps in cell death, all of which could occur without mitotic division (*33–35*), before concluding that the labeled cells are newly generated neurons. Our results are in harmony with previous ^{3}H-TdR autoradiographic studies in both primate and nonprimate species, indicating that neurogenesis of the neocortex is normally confined to developmental periods (*3–10*, *12*, *13*). Consistent with our findings, a recent study with immunofluorescent double-labeling of cortical cells with BrdU and NeuN in adult mice also failed to detect neurogenesis under normal conditions (*36*).

Finally, the negative findings in the present study cannot be attributed to inadequate histological processing because we could positively identify adult-generated neurons colabeled for BrdU and NeuN in the hippocampal dentate gyrus and olfactory bulb in the very animals examined for cortical neurogenesis (Fig. 3) (*20*, *21*). Moreover, we could identify immature BrdU/TuJ1 double-stained neuroblasts in the SVZ and olfactory tract that migrate to the olfactory bulb (see Fig. 3) (*21*) as they do in other mammalian species (*17*, *37*, *38*). However, we did not detect any migrating neuroblasts entering the overlying subcortical white matter, by using double-staining for BrdU and TuJ1 (*39*). We did observe BrdU-labeled cells in the subcortical white matter, but these were not arrayed in the migratory stream from the SVZ to the prefrontal principal sulcus as diagrammed in Fig. 4 in Gould *et al.* (*22*). Rather, in our material, these cells were distributed throughout the white matter along blood vessels or along myelinated fiber tracts, typical of newly generated endothelial cells and oligodendrocytes, respectively, which have also been observed in numerous previous studies (*11–13*, *28–32*, *40–46*). The aligned rows of cells identified as chains of migratory neurons in Fig. 5D of Gould *et al.* (*22*) and Fig. 4C of their subsequent paper (*24*) appear to be endothelial cells lining a longitudinally cut capillary. The cytological features used previously to identify BrdU-labeled cells as migrating neurons in the

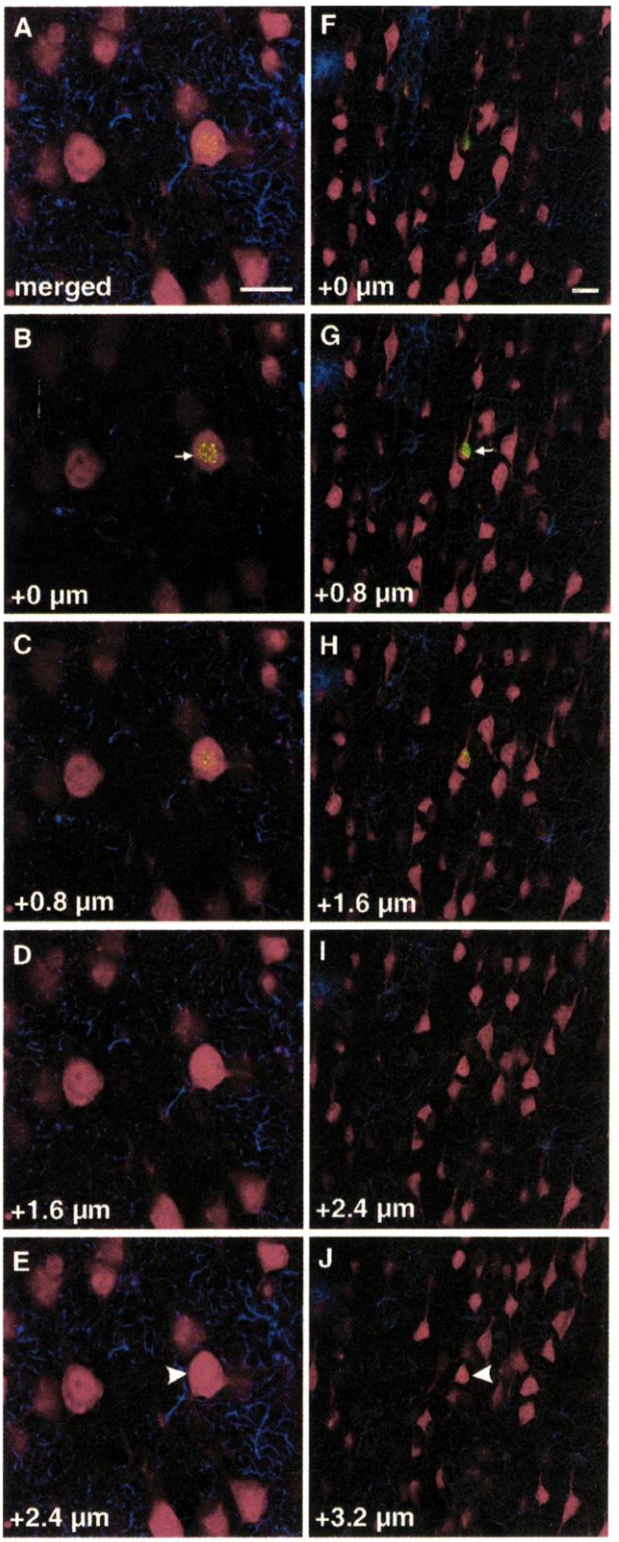

Fig. 2. Images of cells in the adult macaque monkey prefrontal cortex that appear to be double-labeled for BrdU and NeuN are instead resolved to be two closely apposed single-labeled cells. (**A**) A NeuN-positive neuron (red) appeared to be colabeled with BrdU (green) in a merged image. However, a z-series analysis (**B** to **E**) revealed that the BrdU-labeled nucleus (arrow) was located in a different focal plane than the NeuN-positive neuronal cell body. The BrdU-positive nucleus is visible in (B) and (C), and the NeuN-positive nucleus and nucleolus are visible in (D) and (E) (arrowhead), demonstrating that the neuron is not BrdU-labeled. (**F** to **J**) An example of a pyramidal neuron that appears to be BrdU-labeled in sections [(F) to (H), arrow] is shown to have its nucleus and nucleolus in a different focal plane [(I) and (J), arrowhead]. These BrdU-labeled nuclei apparently belong to adult-generated satellite glia, which typically associate with neuronal perikarya (see Fig. 1). Astrocytes are indicated by GFAP immunoreactivity (blue). Scale bars, 20 μm.

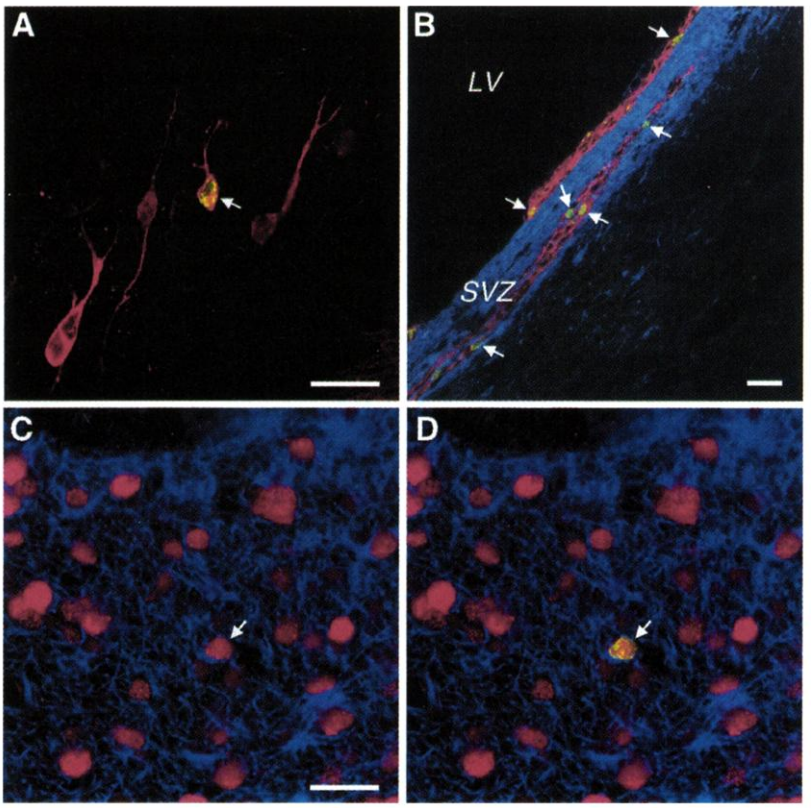

Fig. 3. Newly generated cells with neuronal characteristics in the adult macaque monkey brain. (**A** and **B**) Immature neurons expressing TuJ1 (red) are distributed in the SVZ along the lateral and ventrobasal walls of the lateral cerebral ventricle. BrdU-labeled nuclei (greenish-yellow; arrows) indicate that these are newly generated cells. (A) Immature morphology and the colocalization of BrdU within the nuclei of TuJ1-labeled neuroblasts. (B) Neuroblasts in the SVZ coalesce into migratory chains that extend via the rostral migratory stream to the olfactory bulb. Migrating neuroblasts were not observed in the subcortical white matter. Ependymal and astrocytic cells are indicated by GFAP (blue). LV, lateral ventricle. (**C** and **D**) An example of a newly generated granule cell in the olfactory bulb that is colabeled for NeuN [arrow, red in (C)] and BrdU [arrow, yellow-green in (D)]. A z-stack series through this cell (*56*) revealed that the BrdU signal is confined within and coextensive with the NeuN-labeled nucleus of the cell. Scale bars, 20 μm.

adult macaque [i.e., bipolar morphology and colabeling for CRMP-4 (collapsin response-mediated protein 4; also named TUC-4/Ulip1, formerly "TOAD-64")] (*22*) are also exhibited by cells in the oligodendrocyte lineage (*43*, *44*). Thus, these criteria cannot be used to identify BrdU-labeled cells in the white matter as migrating neurons. A more detailed discussion of the caveats of the methods used, as well as a critique of the specific aspects of the previous studies, is provided elsewhere (*27*, *28*).

The present findings lead to the conclusion that neocortical neurons are not normally renewed during the life-span of macaque monkeys, which can last three decades (*13*); similar limits may exist in the human forebrain (*47*). Although preservation of neurons during one's life-span is considered important for the storage of memory and life-long experience (*13*), the decreased capacity for neurogenesis in adulthood may be an impediment when the need arises for replacement of lost neurons in trauma and neurodegenerative disorders (*48*). The challenge in the coming years will be to determine how to replace lost neurons in brain regions where they are normally not renewed and how to incorporate them into an adult brain environment to restore lost function (*36*, *37*, *49*–*54*).

References and Notes

1. E. R. Kandel, J. H. Schwartz, T. M. Jessel, *Principles of Neuroscience* (McGraw-Hill, New York, 1991).
2. M. S. Gazzaniga, Ed., *Cognitive Neuroscience* (MIT Press, Cambridge, MA, 1999).
3. J. B. Angevine Jr., R. L. Sidman, *Nature* **192**, 766 (1961).
4. C. A. Jackson, J. D. Peduzzi, T. L. Hickey, *J. Neurosci.* **9**, 1242 (1989).
5. S. P Hicks, C. J. D'Amato, *Anat. Rec.* **160**, 619 (1968).
6. V. S. Caviness Jr., R. L. Sidman, *J. Comp. Neurol.* **148**, 141 (1973).
7. P. Rakic, *Science* **183**, 425 (1974).
8. G. Bruckner, V. Mares, D. Biesold, *J. Comp. Neurol.* **166**, 245 (1976).
9. I. H. M. Smart, M. Smart, *J. Anat.* **134**, 273 (1982).
10. M. B. Luskin, C. J. Shatz, *J. Comp. Neurol.* **242**, 611 (1985).
11. H. Korr, B. Schultze, W. Mauer, *J. Comp. Neurol.* **150**, 169 (1973).
12. V. Mares, G. Bruckner, *J. Comp. Neurol.* **177**, 519 (1978).
13. P. Rakic, *Science* **227**, 1054 (1985).
14. R. S. Nowakowski, S. B. Lewin, M. W. Miller, *J. Neurocytol.* **18**, 311 (1989).
15. G. Kempermann, H. G. Kuhn, F. H. Gage, *Proc. Natl. Acad. Sci. U.S.A.* **94**, 10409 (1997).
16. E. A. Markakis, F. H. Gage, *J. Comp. Neurol.* **406**, 449 (1999).
17. V. Coskun, M. B. Luskin, *J. Neurosci.* **21**, 3092 (2001).
18. P. S. Eriksson *et al.*, *Nature Med.* **4**, 1313 (1998).
19. E. Gould *et al.*, *Proc. Natl. Acad. Sci. U.S.A.* **96**, 5263 (1999).
20. D. R. Kornack, P. Rakic, *Proc. Natl. Acad. Sci. U.S.A.* **96**, 5768 (1999).
21. ———, *Proc. Natl. Acad. Sci. U.S.A.* **98**, 4752 (2001).
22. E. Gould, A. J. Reeves, M. S. Graziano, C. G. Gross, *Science* **286**, 548 (1999).
23. E. Gould, C. G. Gross, *Science* **288**, 771a (2000) [summary] (full text available on *Science* Online at www.sciencemag.org/cgi/content/full/288/5467/771a).
24. E. Gould, N. Vail, M. Wagers, C. G. Gross, *Proc. Natl. Acad. Sci. U.S.A.* **98**, 10910 (2001).
25. A total of 10 adult male and nonpregnant female macaque monkeys, over 5 years of age, received intravenous injections of BrdU (Sigma) dissolved in 0.9% NaCl with 0.007 M NaOH. Four cynomolgus macaques (*Macaca fascicularis*) received five consecutive daily injections of BrdU (50 mg of BrdU per kg of body weight per injection) and were perfused 2 hours or 12, 31, or 75 days after the final injection; another *M. fascicularis* was perfused 2 hours after only one BrdU injection. Brains were processed for BrdU peroxidase immunohistochemistry and were used to follow the regional distribution of BrdU-labeled cells after short, intermediate, and long postinjection survival times. Another five monkeys (*M. mulatta*) were processed for triple-label fluorescence immunohistochemistry, after the indicated injection/survival schedules: One monkey was perfused 10 days after four consecutive daily injections (100 mg/kg); one monkey was perfused 23 days after the last of two injections, 5 days apart (75 mg/kg); and three monkeys were perfused 32, 75, or 97 days after the final of five daily injections (75 mg/kg). Supplementary details on animals and experimental procedures are available on Science *Online* at www.sciencemag.org/cgi/content/full/294/5549/2127/DC1.
26. H. G. Kuhn *et al.*, *J. Neurosci.* **17**, 5820 (1997).
27. R. S. Nowakowski, N. L. Hayes, *Science* **288**, 771a (2000) [summary] (full text available on *Science* Online at www.sciencemag.org/cgi/content/full/288/5467/771a).
28. P. Rakic, *Nature Rev. Neurosci.*, in press.
29. K. W. G. McDemott, P. L. Lantos, *Dev. Brain Res.* **57**, 269 (1990).
30. P. Rakic, D. R. Kornack, *Restor. Neurol.* **6**, 257 (1993).
31. S. K. Ludwin, *Nature* **308**, 274 (1984).
32. S. W. Levison, G. M. Young, J. E. Goldman, *J. Neurosci. Res.* **57**, 435 (1999).
33. R. Neve, D. L. McPhie, Y. Chen, *Brain Res.* **886**, 54 (1999).
34. Y. Yang, D. S. Geldmacher, K. Herrup, *J. Neurosci.* **21**, 2661(2001).
35. A. Coponi, *Trends Neurosci.* **24**, 25 (2001).
36. S. S. Magavi, B. R. Leavitt, J. D. Macklis, *Nature* **405**, 951 (2000).
37. F. Doetsch, A. Alvarez-Buylla, *Proc. Natl. Acad. Sci. U.S.A.* **93**, 14895 (1996).
38. L. B. Thomas, M. A. Gates, D. A. Steindler, *Glia* **17**, 1 (1996).
39. The BrdU-labeled cells we observed in the adult macaque SVZ were distributed predominantly along the lateral and ventrobasal walls of the lateral ventricle (*21*), as described in previous studies in rodents and primates [see (*11*–*13*, *18*, *28*–*32*, *40*, *55*)]. In contrast, the BrdU-labeled SVZ cells illustrated in Fig. 4 of Gould *et al.* (*22*) are concentrated in the dorsomedial wall of the lateral ventricle, under the corpus callosum. The reason for this discrepancy in regional distribution is presently unclear.
40. P. Rakic, *Ann. N. Y. Acad. Sci.* **457**, 193 (1985).
41. N. S. Roy *et al.*, *J. Neurosci.* **19**, 9986 (1999).
42. H. Korr, *Adv. Anat. Embryol. Cell Biol.* **61**, 1 (1980).
43. A. Kakita, J. E. Goldman, *Neuron* **23**, 461 (1999).
44. J. Nacher, D. R. Rosell, B. S. McEwen, *J. Comp. Neurol.* **424**, 628 (2000).
45. A. Nishiyama, A. Chang, B. D. Trapp, *J. Neuropathol. Exp. Neurol.* **58**, 1113 (1999).
46. A. Chang, A, Nishiyama, J. Peterson, J. Prineas, B. D. Trapp, *J. Neurosci.* **20**, 6404 (2000).

47. L. Seress, H. Abraham, T. Tornoczky, Gy. Kosztolanyi, *Neuroscience* **105**, 831 (2001).
48. P. Rakic, *Nature Neurosci.* **1**, 643 (1998).
49. B. Kirschenbaum *et al.*, *Cereb. Cortex* **4**, 576 (1994).
50. F. Doetsch, I. Caille, D. A. Lim, J. M. Garcia-Verdugo, A. Alvarez-Buylla, *Cell* **97**, 703 (1999).
51. F. H. Gage, *Science* **287**, 1433 (2000).
52. E. D. Laywell, P. Rakic, V. G. Kukekov, E. C. Holland, D. A. Steindler, *Proc. Natl. Acad. Sci. U.S.A.* **97**, 13883 (2000).
53. A. Bjorklund, O. Lindvall, *Nature Neurosci.* **3**, 537 (2000).
54. R. McKay, *Nature* **406**, 361 (2000).
55. A. Privat, *Int. Rev. Cytol.* **40**, 281 (1975).
56. D. R. Kornack, P. Rakic, data not shown.
57. We thank P. S. Goldman-Rakic, E. A. Markakis, and N. Sestan for insightful comments. Supported by grants NS14841 and EY02593 from the United States Public Health Service.

17 August 2001; accepted 24 October 2001

Persistent Solar Influence on North Atlantic Climate During the Holocene

Gerard Bond,[1]* Bernd Kromer,[2] Juerg Beer,[3] Raimund Muscheler,[3] Michael N. Evans,[4] William Showers,[5] Sharon Hoffmann,[1] Rusty Lotti-Bond,[1] Irka Hajdas,[6] Georges Bonani[6]

Surface winds and surface ocean hydrography in the subpolar North Atlantic appear to have been influenced by variations in solar output through the entire Holocene. The evidence comes from a close correlation between inferred changes in production rates of the cosmogenic nuclides carbon-14 and beryllium-10 and centennial to millennial time scale changes in proxies of drift ice measured in deep-sea sediment cores. A solar forcing mechanism therefore may underlie at least the Holocene segment of the North Atlantic's "1500-year" cycle. The surface hydrographic changes may have affected production of North Atlantic Deep Water, potentially providing an additional mechanism for amplifying the solar signals and transmitting them globally.

A prominent feature of the North Atlantic's Holocene climate is a series of shifts in ocean surface hydrography during which drift ice and cooler surface waters in the Nordic and Labrador Seas were repeatedly advected southward and eastward, each time penetrating deep into the warmer strands of the subpolar circulation (*1*, *2*). The persistence of those rather dramatic events within a stable interglacial has been difficult to explain. Earlier work (*3*) suggested that a low-resolution record of North Atlantic drift ice in the early Holocene may have been linked to the energy output of the Sun. The likelihood of any such strong climate response to solar variability has long been debated because the magnitude of the forcing is small. Results of recent atmospheric general circulation (GCM) mod-

[1]Lamont-Doherty Earth Observatory of Columbia University, Route 9W, Palisades, NY 10964, USA. [2]Heidelberg Academy of Sciences, Institute of Environmental Physics, INF 229, D-69120 Heidelberg, Germany. [3]Eidgenössische Anstalt für Wasserversorgung, Abwasserreinigung und Gewuässerschutz, Ueberlandstrasse 133, Postfach 611, CH-8600 Duebendorf, Switzerland. [4]Laboratory of Tree-Ring Research, University of Arizona, 105 West Stadium, Tucson, AZ 8572, USA. [5]Department of Marine, Earth and Atmospheric Sciences, North Carolina State University, 1125 Jordan Hall, Raleigh, NC 27695–8208, USA. [6]Accelerator Mass Spectrometry ^{14}C Lab, ITP Eidgenössische Technische Hochschule Hoenggerberg, CH-8093 Zurich, Switzerland.

*To whom correspondence should be addressed. E-mail: gcb@ldeo.columbia.edu

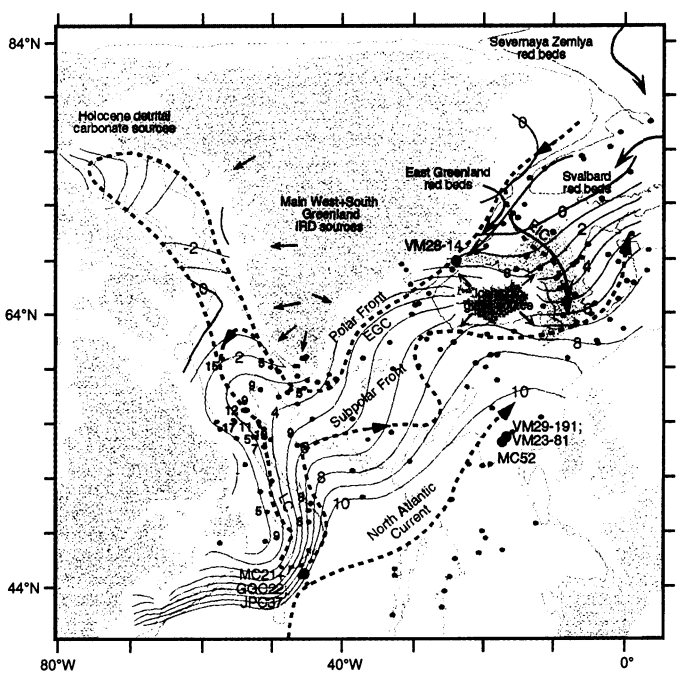

Fig. 1. Map of coring sites described in the text that provide the basis for inferring sources and transport routes of ice carrying the petrologic tracers. Dashed blue lines: subpolar cyclonic circulation. The main frontal boundaries are labeled in blue. Red dots are core-top measurements of all tracers. Areas enclosed by shading indicate core tops with >10% of tracers as keyed by colors [red: >10% hematite-stained grains (HSG); yellow: >10% Icelandic glass (IG); blue: >10% detrital carbonate (DC)]. Documentation for core-top percentages of HSG and IG are from (*2*); red numbers next to core-top locations are percentages of DC in core tops. Colored arrows indicate inferred direction of transport of tracer-bearing drift ice. Gray lines are mean (1900 to 1992) ocean-surface temperatures from LEVITUS94 (*52*) for spring when iceberg discharge into the North Atlantic reaches a maximum. EIC: East Iceland Current; EGC: East Greenland Current; LC: Labrador Current. VM28-14: 64°47′N, 29°34′W, 1855-m water depth; VM29-191: 54°16′N, 16°47′W, 2370-m water depth; VM23-81: 54°15′N, 16°50′W, 2393-m water depth; KN158-4 MC52: 55°28′N, 14°43′W, 2172-m water depth; KN158-4 MC21, KN158-4 GGC22: 44°18′N, 46°16′W, 3958-m water depth; and EW9303 JPC37: 43°58′N, 46°25′W, 3980-m water depth. Petrologic analyses of more than 120 core tops demonstrates that most tracer-bearing ice today circulates in the cooler waters north and west of the subpolar front. Lower tracer percentages to the south and east are consistent with observational evidence that icebergs there come mainly from south and west Greenland where tracer-bearing rock types are rare, if present at all. Increases in DC off Newfoundland, therefore, reflect southward shifts of the cooler Labrador Sea surface water and carbonate-bearing drift ice. Peak percentages of HSG and IG off Newfoundland rarely reach the corresponding peak values of those two tracers in the eastern North Atlantic (MC52-VM29-191) (Fig. 2). That rules out transport of HSG and IG through the East Greenland–Labrador Sea current system at times of peak drift-ice transport. The eastern North Atlantic drift-ice records, therefore, require that at times of peak tracer percentages, ice-bearing surface waters from north of Iceland were advected southeastward toward the coring site. That was accompanied by cooler ocean-surface temperatures (*1*) and, by analogy with transport mechanisms of modern drift ice (*53*), must have been aided by northerly or northeasterly surface winds in the Nordic Seas and eastern subpolar North Atlantic. The concentrations of IRD (lithic grains >150 μm), although small, covary with the petrologic tracers, and peak percentages reflect true increases in the tracer concentrations rather than dilution by other grain types.